Quaternion Markov Splicing Detection for Color Images Based on Quaternion Discrete Cosine Transform

Jinwei Wang[1,2,3*], Renfeng Liu[1], Hao Wang[1] , Bin Wu[4] and Yun-Qing Shi[5]

[1] School of Computer and Software, Nanjing University of Information Science and Technology, Jiangsu, 210044, China

[2]State Key Laboratory of Information Security (Institute of Information Engineering, Chinese Academy of Sciences, Beijing 100093)

[3]Shaanxi Key Laboratory of Network and System Security, Xidian University, Xi'an, Shaanxi 710071, China

[4]Institute of Information Engineering, Chinese Academy of Sciences

[5] Department of Electrical and Computer Engineering, New Jersey Institution of Technology, NJ, 07102, USA

*Corresponding author: Jinwei Wang

E-mail : wjwei_2004@163.com

Received February 9, 2020; revised June 24, 2020; accepted July 19, 2020; published July 31, 2020

Abstract

With the increasing amount of splicing images, many detection schemes of splicing images are proposed. In this paper, a splicing detection scheme for color image based on the quaternion discrete cosine transform (QDCT) is proposed. Firstly, the proposed quaternion Markov features are extracted in QDCT domain. Secondly, the proposed quaternion Markov features consist of global and local quaternion Markov, which utilize both magnitude and three phases to extract Markov features by using two different ways. In total, 2916-D features are extracted. Finally, the support vector machine (SVM) is used to detect the splicing images. In our experiments, the accuracy of the proposed scheme reaches 99.16% and 97.52% in CASIA TIDE v1.0 and CASIA TIDE v2.0, respectively, which exceeds that of the existing schemes.

Keywords: splicing detection, color image, QDCT, quaternion Markov

This work was supported in part by the Natural Science Foundation of China under Grants (Nos. 61702235, 61772281, U1636117, U1636219, 61502241, 61272421, 61232016, 61402235, 61572258 and 61702235), in part by the National Key R&D Program of China(Grant No. 2016YFB0801303 and 2016QY01W0105), in part by the plan for Scientific Talent of He nan Province (GrantNo.2018JR0018),in part by the Natural Science Foundation of Jiangsu Province, China under Grant BK20141006, and the PAPD fund. State Key Laboratory of Information Security (Institute of Information Engineering, Chinese Academy of Sciences, Beijing 100093). Shanxi Key Laboratory of Network and System Security, Xidian University, Xi'an, Shaanxi 710071, China.

http://doi.org/10.3837/tiis.2020.07.014 **ISSN : 1976-7277**

1. Introduction

With the development of image processing technology, the cost of image forensics software is decreasing which destroys the trustworthiness of digital images[1]. Some image forensics issues have been proposed [2]-[7]. Besides, machine learning is used to solve forensics issues [8]-[10]. In forensics issues, splicing operation is a popular tampering method existed in our life, which may cause serious consequences in some cases, such as journalism, judicial investigation, and accident survey. It is very easy to manipulate images with image editing software such as Photoshop, while it is difficult for human being to distinguish the authentic images from splicing images. Therefore, to classify the authentic images, many detection methods of splicing images have been developed.

Image splicing is a common means in image tampering, which is a simple process of cutting and pasting parts of one image or different images to form a forged image. The process includes some post-processing such as Gaussian blur [11]. There are many existing splicing detection schemes, which mainly consist of two categories. One is to extract local features such as blur of the image, inconsistency between the spliced and the authentic regions. In [11]-[15], blur of the image is utilized to detect the splicing images. Documents [16]-[19] make use of neighbour graylevel between the spliced regions and the authentic images. This kind of schemes can not only distinguish splicing images from authentic images, also find the spliced regions. However, the classification accuracy of these schemes is not as high as the other category of schemes.

The other is to extract global features to classify the images. In [20] and [21], higher-order statistical characteristics of wavelet transform was used to reflect the inherent characteristics of natural images. It laid a foundation for many similar methods. In [22], a scheme based on the moments feature and Markov transition probability is proposed. In [23], gray level co-occurrence matrix is regarded as the classification features for splicing detection. In [24], a natural image model is presented based on Markovian rake transform on image luminance. In [25], a scheme based on Markov features in DCT (Discrete Cosine Transform) and DWT (Discrete Wavelet Transform) is proposed. These schemes cannot find the spliced regions, but they have higher classification accuracy than the first category. Our proposed scheme belongs to the second category.

In the last few years, many schemes are proposed [26]-[34]. Some of them have reached the high accuracy which is over 95%. In [26], Markov features based on spatial and DCT domain are combined for image splicing, the accuracy of which reaches 98.47% in the Columbia Image Splicing Detection Evaluation Dataset (CISDED) [28]. CISDED is not adopted in our experiments because the sample number of color images in this database is too small. Splicing detection based on Markov features in QDCT domain is proposed in [29]. The accuracy arrives at 96.44% in CASIA TIDE v1.0 [30]. In [31], local binary features based on SPT (Steerable Pyramid Transform) domain is extracted for classification. The accuracy reaches 97.33% in CASIA TIDE v2.0. In [32], features based on DCT and Contourlet transform domain are used for splicing detection. The accuracy arrives at 96.69% in an international competition organized by the IEEE IFS-TC. In [33], a new image forgery detection method based on deep learning technique is presented. The accuracy arrives at 98.04% in CASIA TIDE v1.0 and 97.83% in v2.0.

Most of the existing methods transform color images into grayscale images or utilize one part of RGB channels. Therefore, the inherent relationship among RGB channels is neglected.

In this paper, we propose to extract features in QDCT domain and three imaginary parts of the quaternion is utilized to represent of RGB channels, respectively. Color image as a unit is processed. In contrast to [29], the proposed scheme makes full use of both the magnitude and three phases to extract Markov features. In experiments, the proposed scheme has better performance.

The rest of this paper is organized as follows. In Section 2, the quaternion and block QDCT are introduced. The proposed quaternion Markov is presented, and the quaternion Markov is composed of global quaternion Markov and local quaternion Markov. After presenting the proposed scheme, the experimental results and discussion are shown in Section 3. Section 4 draws a conclusion of this paper.

2. The Proposed Scheme

2.1. Introduction to QDCT

DCT has been widely used in image processing due to its superior capability in decorrelation and energy compaction. QDCT is extended from DCT. Therefore, compared with DCT, QDCT not only owns the similar function as DCT but obtains the channel correlation and color information of color images. As a result, features extracted in QDCT domain have more efficient information to promote the performance of the proposed scheme.

2.1.1. Quaternion

The quaternion is proposed by Hamilton in 1843 in [35]. A quaternion is composed of one real part and three imaginary parts. The quaternion is formed as.

$$q = a + b\boldsymbol{i} + c\boldsymbol{j} + d\boldsymbol{k} \tag{1}$$

, where a, b, c, d ∈ **R**.i, j, k obey the following constraints:

$$\boldsymbol{i}^2 = \boldsymbol{j}^2 = \boldsymbol{k}^2 = -1 \tag{2}$$

$$\boldsymbol{ij} = -\boldsymbol{ji} = \boldsymbol{k}, \boldsymbol{jk} = -\boldsymbol{kj} = \boldsymbol{i}, \boldsymbol{ki} = -\boldsymbol{ik} = \boldsymbol{k} \tag{3}$$

From Eq. (3), we can observe that the commutative of the quaternion doesn't meet the law of multiplication. The magnitude of a quaternion is defined as follows:

$$|q| = \sqrt{a^2 + b^2 + c^2 + d^2} \tag{4}$$

A polar form of the quaternion is composed of the magnitude and three angles (φ, θ, ψ) called phase. The equation is written as follows:

$$q = |q|e^{\boldsymbol{i}\varphi}e^{\boldsymbol{j}\boldsymbol{\theta}}e^{\boldsymbol{k}\psi} \tag{5}$$

$$\varphi = \frac{atan\big(2(cd + ab), (a^2 - b^2 + c^2 - d^2)\big)}{2} + k\pi \tag{6}$$

$$\theta = \frac{atan\big(2(bd + ac), (a^2 + b^2 - c^2 - d^2)\big)}{2} \tag{7}$$

$$\psi = \frac{arcsin\big(2(ad - bc)\big)}{2} \tag{8}$$

, where $\varphi \in [-\pi, \pi]$, $\theta \in [-\pi/2, \pi/2]$, $\psi \in [-\pi/4, \pi/4]$, k ∈ Z. Referred to [36], the magnitude and three angles are used to represent QDCT coefficients in the proposed scheme. Usually, we consider a quaternion composed of a scalar and vector part as follows:

$$q = S(q) + V(q) \tag{9}$$

, where $S(q) = a$ and $V(q) = b\boldsymbol{i} + c\boldsymbol{j} + d\boldsymbol{k}$. If $S(q) = 0$, q is called a pure quaternion. If $|q| = 1$, q is called a unit quaternion

2.1.2. Definition of QDCT

QDCT is derived from DCT. The definition of QDCT is referred to [37]. There are two forms of QDCT, L-QDCT, and R-QDCT. This subsection only introduce L-QDCT which are used in the proposed scheme. L-QDCT is as follows:

$$QDCT_q^L(p,s) = a(p)a(s)\sum_{m=0}^{M-1}\sum_{n=0}^{N-1} u_q f_q T(p,s,m,n) \tag{10}$$

, where $f_q(m, n)$ is a M × N quaternion matrix. u_q is a unit and pure quaternion. $QDCT_q^L(p, s)$ is the transformed matrix. p and s are row and column of the obtained matrix, respectively. $\alpha(p)$, $\alpha(s)$ and $T(p, s, m, n)$ are defined as follows:

$$a(p) = \begin{cases} \sqrt{1/M} & p = 0 \\ \sqrt{1/M} & p \neq 0 \end{cases} \quad a(s) = \begin{cases} \sqrt{1/N} & s = 0 \\ \sqrt{1/N} & s \neq 0 \end{cases} \tag{11}$$

$$T(p,s,m,n) = \cos\left[\frac{\pi(2m+1)p}{2M}\right]\cos\left[\frac{\pi(2n+1)s}{2N}\right] \tag{12}$$

There are two ways to calculate QDCT. One of the ways is to calculate QDCT directly with its definition. The other way is to use two complex numbers to represent the quaternion and then compute QDCT with DCT. More details are given in [37].

2.2. The Proposed Scheme

QDCT owns the property of energy concentration. The magnitude of quaternion represents the signal strength and the phases of quaternion depict the structure of the signal. Therefore, features extracted from the magnitude and phases can be used in the proposed scheme.

This section will first illustrate the framework of the proposed scheme briefly and analyze the difference between global and local quaternion Markov. Next, we will describe three threshold processing methods after obtaining the difference arrays of quaternion Markov. Then, six types of transition probability matrix will be introduced. Finally, the calculation steps of global and local quaternion Markov will be presented in detail.

2.2.1. The Framework of the Proposed Scheme

The framework of the proposed scheme is shown in **Fig. 1**. The framework is organized as follows:

1) Use the block QDCT to decompose the color image.
2) Process the QDCT coefficients using the proposed quaternion Markov. The process is presented in **Fig. 2**. The quaternion Markov comprises global quaternion Markov and local quaternion Markov. Framework of global quaternion Markov is presented as follows:

(i) Compute the magnitude and three phases of QDCT coefficients.
(ii) Calculate the difference of the magnitude array and phase arrays in four directions. Process difference arrays with a threshold.
(iii) Obtain the transition probability matrices.

The framework of local quaternion Markov is shown as follows:

(i) Compute the difference of QDCT coefficients in four directions. Process difference arrays with a threshold.
(ii) Get the magnitude and phases of the difference arrays.
(iii) Figure up the transition probability matrices.

3) Transform the transition probability matrices into features. SVMRFE (SVM Recursive Feature Elimination) is used to sort features according to the importance and choose the features for training and testing with SVM. SVMRFE can be referred to [15] for more details.

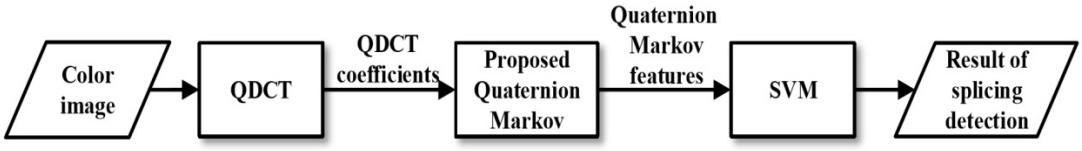

Fig. 1. The framework of the proposed scheme

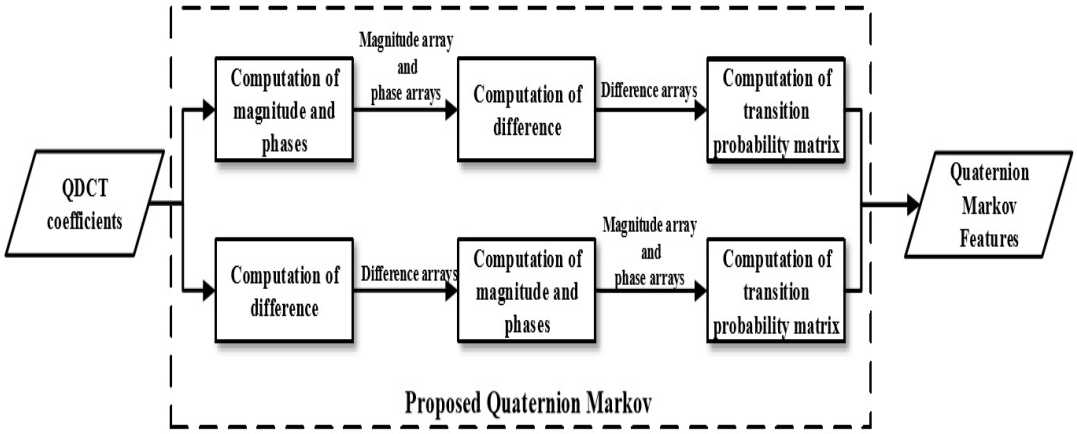

Fig. 2. The proposed Quaternion Markov

The steps of two classes of quaternion Markov are similar, but their functions are different.

In global quaternion Markov, the magnitude array and phase array of QDCT coefficients are firstly computed to obtain strength information and texture information of the whole image. Therefore, Markov features that contain the integral information of QDCT coefficients are called global quaternion Markov. In local quaternion Markov, the difference arrays are firstly calculated and then the magnitude and phases of difference arrays are computed to get difference information of QDCT coefficients. Markov features that contain the difference information are named local quaternion Markov. There is a common difference processing in

both global quaternion Markov and local quaternion Markov. Difference processing in global quaternion Markov is used to reduce the effect caused by the diversity of images, while in local quaternion Markov, difference processing is utilized to reflect the texture of QDCT coefficients.

The procedure of the proposed scheme is briefly described above. The subsection in the following will give the detailed introduction of the proposed quaternion Markov.

2.2.2. Threshold Processing of Difference Arrays

A difference array is obtained by computing the difference of each pair of the neighbors in the array in one direction. By using Equations (13) to (16), difference arrays in four directions (horizontal, vertical, main diagonal and minor diagonal) are obtained

$$F_u(u,v) = F(u,v) - F(u+1,v) \tag{13}$$
$$F_h(u,v) = F(u,v) - F(u,v+1) \tag{14}$$
$$F_d(u,v) = F(u,v) - F(u+1,v+1) \tag{15}$$
$$F_s(u,v) = F(u+1,v) - F(u,v+1) \tag{16}$$

where F denotes the 2-D array, F_u, F_h, F_d and F_s are difference arrays in horizontal, vertical, main diagonal and secondary diagonal directions, respectively. u and v are position of the array F.

In order to decrease computational complexity, threshold processing is conducted on difference arrays. The value scopes of magnitude arrays and phase arrays are different in the proposed scheme, so there are three methods of threshold processing according to **Fig. 2**. Here, x denotes an element in a difference array, and T denotes a threshold.

Method A (MA) It is applied to the difference in global quaternion magnitude. After Computing magnitude of QDCT coefficients and then calculating the difference arrays of the magnitude, we use Eq. (17) to process the difference arrays.

$$x = \begin{cases} T, & if\ x > T \\ x, & if\ -T \le x \le T \\ -T, & if\ x < -T \end{cases} \tag{17}$$

Method B (MB) According to Equation (4), the magnitude is greater than or equal to zero. It is set for magnitude of local quaternion Markov. After computing difference arrays of QDCT coeffi- cients and then calculating the magnitude of the difference arrays, Eq. (18) is used to obtain new difference arrays.

$$x = \begin{cases} T, & if\ x > T \\ x, & if 0 \le x \le T \end{cases} \tag{18}$$

Method C (MC) Pointing to phase feature in global and local quaternion Markov, we utilize Eq. (19) to replace all the elements in a difference array.

$$x = T * \frac{K * x}{\pi}, \quad K = 1,2,4 \tag{19}$$

2.2.3. Transition Probability Matrix

In the proposed scheme, there are six Probability transition matrices, which are calculated by Eq. (20) to (25).

$$P_{hh} = \frac{\sum_{v=0}^{V-2}\sum_{u=0}^{U-2}\delta(F_h(u,v) = a, F_h(u+1,v) = b)}{\sum_{v=0}^{V-2}\sum_{u=0}^{U-2}\delta(F_h(u,v) = a)} \tag{20}$$

$$P_{hh} = \frac{\sum_{v=0}^{V-2}\sum_{u=0}^{U-2}\delta(F_h(u,v)=a, F_h(u,v+1)=b)}{\sum_{v=0}^{V-2}\sum_{u=0}^{U-2}\delta(F_h(u,v)=a)} \quad (21)$$

$$P_{hh} = \frac{\sum_{v=0}^{V-2}\sum_{u=0}^{U-2}\delta(F_v(u,v)=a, F_v(u+1,v)=b)}{\sum_{v=0}^{V-2}\sum_{u=0}^{U-2}\delta(F_v(u,v)=a)} \quad (22)$$

$$P_{hh} = \frac{\sum_{v=0}^{V-2}\sum_{u=0}^{U-2}\delta(F_v(u,v)=a, F_v(u,v+1)=b)}{\sum_{v=0}^{V-2}\sum_{u=0}^{U-2}\delta(F_v(u,v)=a)} \quad (23)$$

$$P_{hh} = \frac{\sum_{v=0}^{V-2}\sum_{u=0}^{U-2}\delta(F_d(u,v)=a, F_d(u+1,v+1)=b)}{\sum_{v=0}^{V-2}\sum_{u=0}^{U-2}\delta(F_d(u,v)=a)} \quad (24)$$

$$P_{hh} = \frac{\sum_{v=0}^{V-2}\sum_{u=0}^{U-2}\delta(F_s(u+1,v)=a, F_s(u,v+1)=b)}{\sum_{v=0}^{V-2}\sum_{u=0}^{U-2}\delta(F_s(u,v)=a)} \quad (25)$$

, where $a, b \in \{-T, -T+1, \cdots, T-1, T\}$ or $\{0, 1, \cdots, T-1, T\}$, U and V denote the row number and column number of the array F , respectively, and

$$\delta(\mathrm{A}=\mathrm{a}, \mathrm{B}=\mathrm{b}) = \begin{cases} 1, & if\ A=a, B=b \\ 0, & otherwise \end{cases} \quad (26)$$

Eq. (20) and (21) are used for horizontal difference arrays, Eq. (22) and (23) are used for vertical difference arrays and Eq. (24) and (25) are used for main diagonal and minor diagonal difference arrays, respectively.

2.2.4. The Proposed Quaternion Markov

Markov feature can reflect the statistical change after image splicing. Therefore, it is adopted in this paper. However, there are some changes in the pro posed quaternion Markov compared to the traditional Markov in [12]. Traditional Markov is only suitable for real field while the proposed quaternion Markov is extended to quaternion. Therefore, its amount of transition probability matrices are different from that of the traditional Markov. The proposed quaternion Markov is presented as follows.

a) Global quaternion Markov is represented in detail. As shown in **Fig. 3**, it is divided into the following steps:
b) A color image is transformed by using the 8×8 block QDCT to obtain QDCT coefficients.
c) Compute the magnitude and three phases of each element of the quaternion array using Eq. (4), (6), (7) and (8). One magnitude array and three phase arrays can be obtained.
d) The difference arrays of magnitude and phase are calculated by using Eq. (13) to (16).
e) Handle the magnitude differences array and the phase difference arrays with threshold processing methods MA and MC, respectively. Therefore, 16 difference arrays are obtained, composed of 4 magnitude arrays and 12 phase arrays.
f) Round these 16 arrays.
g) Figure up the transition probability matrices of these 16 obtained arrays using Eq. (20) to (25).

Note that Eq. (20) to (25) are applied to the magnitude difference arrays and Eq. (20), (22), (24) and (25) are applied to the phase arrays. Therefore, 18 transition probability matrices for 6 matrices of magnitude and for 4 matrices of 3 phases φ, θ and ψ are finally obtained.

Local quaternion Markov is similar to global quaternion Markov. The distinction between two ways is the order of the steps. Local quaternion Markov is shown as follows:

a) It is similar to a) of global quaternion Markov.
b) Calculate the difference arrays of the quaternion array with Eq. (13) to (16) which is different from b) of global quaternion Markov.
c) The magnitude and three phases of each element of four difference array are computed. 16 difference arrays are obtained, composed of 4 magnitude and 12 phase arrays by using Eq. (4), (6), (7) and (8).
d) Handle the magnitude differences array and the phase difference arrays with threshold processing methods MB and MC.
e) Round these 16 arrays.
f) The transition probability matrices of these 16 arrays are obtained by using Eq. (20) to (25).

The computation of transition probability matrices in Local quaternion Markov is similar to that in Global quaternion Markov.

In total,there are 36 transition probability matrices obtained in the proposed quaternion Markov.

3. Experiments

To evaluate the performance of the proposed scheme, we conduct a series of experiments referred to [38] and [39]. The experimental results show the high accuracy of the proposed scheme. In this section, we will first introduce the image database used in our experiments. Then, the components of the features and the experiment al results are presented. Next, the choice of T will be discussed. At last, the comparison between the proposed scheme and the existing schemes are shown.

3.1. Introduction to Database

Due to the splicing detection for color image in the proposed scheme, the database should consist of color image. However, the database in [28] is too small number of color image to be adopted in this experiment. CASIA TIDE v1.0 and CASIA TIDE v2.0 are finally selected. CASIA TIDE v1.0 consists of 800 authentic images and 921 splicing images. The size of the images in this database is 384×256 pixels in the format of JEPG. CASIA TIDE v2.0 is composed of 7491 authentic images and 5123 splicing images. The size of the images in this database is from 240×160 to 900×600 pixels in the format of JEPG, BMP and TIFF. In our experiments, the image database is randomly divided into two halves, one half for training and the other for testing. Some samples which chosen from CASIA TIDE v1.0 and v2.0 are shown in **Fig. 3** and **Fig. 4**. In both figures, the first row shows authentic images and the second row shows splicing images.

Fig. 3. Samples of CASIA TIDE v1.0

Fig. 4. Samples of CASIA TIDE v2.0

3.2. Feature Generation and Performance Evaluation

In our experiments, features are divided into four sets and listed as follows:

a) Set1: Features from the magnitude array in global quaternion Markov. $(2 \times T_1 + 1)^2 \times 6 - D$ ($-D$ denotes the dimensionality) features can be obtained from this set.

b) Set2: Features are derived from the phase arrays in global quaternion Markov. $(2 \times T_2 + 1)^2 \times 12 - D$ features can be gotten from this set.

c) Set3: Features root in the magnitude arrays in local quaternion Markov. $(2 \times T_3 + 1)^2 \times 6 - D$ features can be obtained from this set.

d) Set4: Features in this set result from the phase arrays in local quaternion Markov. $(2 \times T_4 + 1)^2 \times 12 - D$ features can be computed.

In our experiments, we set the thresholds of the four sets as 4, 4, 8 and 4, respectively. The reason will be discussed in the following subsection. Therefore, there are 2916-D features totally

The 2916-D features bring many redundant features, which are composed of four sets. As a result, before presenting the performance of features, SVMRFE is used to sort the features according to their importance. After sorting the obtained features, we select the first hundreds of features and leave the rest of features. Finally, SVM is used for training and testing the images and the average accuracy of 5 echoes is adopted. It takes average 2.4331 seconds for an image in CASIA TIDE v2.0 to be classified, including feature extraction time and classification time.

Table 1. The experiments of 4 sets with database CASIA TIDE v1.0

dimensionality	100	200	300
Set1	98.72%	98.79%	98.87%
Set2	79.76%	80.05%	80.59%
Set3	95.45%	95.49%	96.03%
Set4	89.77%	91.29%	89.85%
Set1+2	98.75%	98.45%	98.29%
Set3+4	95.96%	97.20%	96.42%
Set1+3	98.85%	98.93%	98.66%
Set2+4	91.43%	92.52%	92.88%
Set1+2+3+4	**99.02%**	**99.16%**	**99.14%**

In **Table 1** and **Table 2**, the experiments of features in four sets and their feature combination are shown. In our experiments, it is found that the accuracy of the proposed scheme is 99.16% in CASIA TIDE v1.0 and 97.52% in CASIA TIDE v2.0 when the dimensionality equals 200. The performance of 100-D, 200-D and 300-D features is shown in **Table 1** and **Table 2**.

Table 2. The experiments of 4 sets with database CASIA TIDE v2.0

dimensionality	100	200	300
Set1	95.77%	96.15%	96.25%
Set2	95.04%	95.38%	94.95%
Set3	95.56%	95.48%	95.32%
Set4	95.67%	96.04%	95.91%
Set1+2	96.54%	96.78%	96.87%
Set3+4	95.70%	96.18%	96.19%
Set1+3	96.47%	96.28%	95.89%
Set2+4	95.89%	96.44%	96.26%
Set1+2+3+4	**97.04%**	**97.52%**	**97.27%**

Table 3. The weight ratio of four sets in 200 selected features

	Set1	Set2	Set3	Set4
CASIA TIDE v1.0	**33%**	17.5%	21.5%	28%
CASIA TIDE v2.0	22.5%	27.5%	15%	**35%**

There are two issues to be discussed in **Table 1** and **Table 2**. The first issue is on the performance difference of magnitude and phase features between **Table 1** and **Table 2**. In **Table 1**, it is obvious that the performance of magnitude features is better than that of phases features, while in **Table 2**, the performance of magnitude features and phase features is almost the same. The second issue is that the classification performance in **Table 1** is higher than that in **Table 2**. They result from the different formats of the images between two databases. CASIA TIDE v1.0 consists of color images with the single JPEG format while CASIA TIDE v2.0 consists of images with JPEG, BMP and TIFF , three different formats. JPEG uses DCT to compress images, which has the property of energy concentration. The magnitude of QDCT represents the information strength, which means energy distribution features. The phases of QDCT depict the structure information, which means texture features. Therefore, the classification performance of magnitude features is better than that of phase features in CASIA TIDE v1.0. Meanwhile, the proposed scheme is based on QDCT, so the different formats of the images between two databases result in the second issue.

The distribution of 200 selected features are shown in **Table 3**. There are two conclusions can be drawn from **Table 3**. They are shown as follows:

a) The ratio of magnitude features (Set1+Set3) to phases features (Set2+Set4) in CASIA TIDE v1.0 is near to 1:1 while the ratio in CASIA TIDE v2.0 is over 1:1.5. The phenomenon indicates that magnitude features are more suitable for detecting JEPG images than phase features.
b) From CASIA TIDE v1.0 to CASIA TIDE v2.0, the ratio of Set1 to Set2 is from over 1.5:1 to less than 1 and the ratio of Set3 to Set4 is from about 1:1 to less than 1:2. It manifests that with the amount of the formats increasing, the importance of phase features improves.

3.3. Impact of Different Thresholds on Accuracy

An issue about the threshold will be discussed in this subsection. In our experiments, there is a positive correlation between the computational work and the value of threshold. Therefore, the value of the threshold is limited. After threshold processing A or C, the value is limited from −T to T. After threshold processing B, the value is limited from 0 to T. For convenience, we set $T_1 = T_2 = \frac{T_3}{2} = T_4$. If T is bigger than 4, it takes significantly bigger time, but accuracy dose not increase much. Therefore, T is set smaller than 5. According to **Table 1** and **Table 2**, the feature dimensionality is set 200- D. The contrastive experiments with different thresholds in CASIA TIDE v2.0 have been done and the results are shown in **Table 4**. In **Table 4**, it is found that the accuracy of the proposed scheme reaches the highest when T equals 4. Therefore, the thresholds of four sets are set as 4, 4, 8, and 4.

To further prove the validity of selected thresholds, a set of experiments are conducted. T_1, T_2, $\frac{T_3}{2}$ and T_4 change from 1 to 4. In order to show the trend of the accuracy, we only show **Fig. 4**, in which T_1 and T_2 are set as 4 and 4, respectively. It is easily judged in **Fig. 5** that the selected thresholds are right.

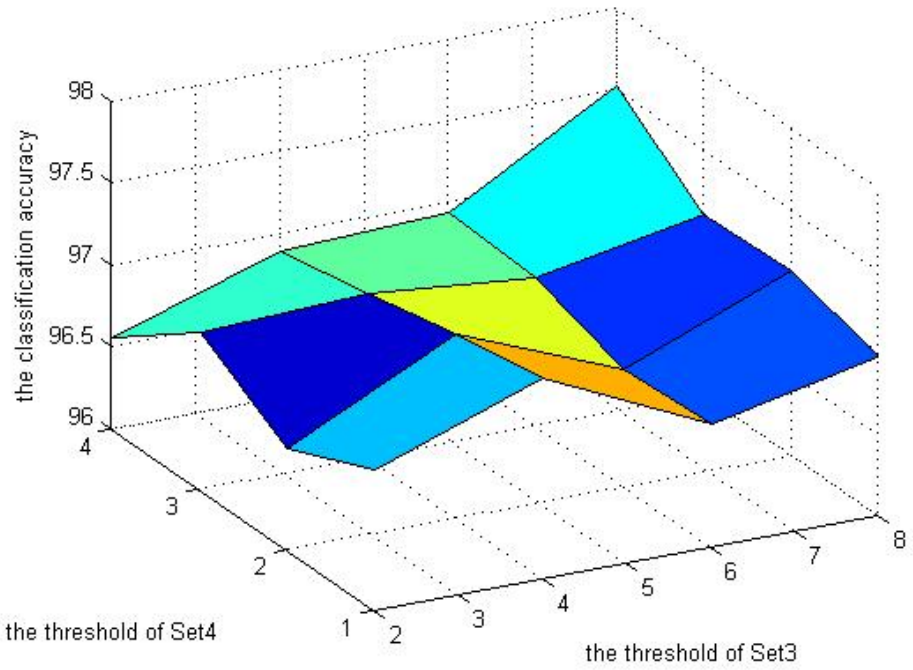

Fig. 5. Experimental results of the classification accuracy with different thresholds of Set3 and Set4

Table 5. The comparison of the proposed scheme with the existing schemes

	accuracy in CASIA TIDE v1.0	accuracy in CASIA TIDE v2.0
He[25]	-	89.76%
Li[29]	96.44%	92.69%
Muhammad [31]	94.89%	97.33%
Zhao[40]	94.70%	-
Rao[33]	98.04%	**97.83%**
Proposed scheme	**99.16%**	97.52%

3.4. Comparison Experiment

In this subsection, the comparison results between the proposed scheme and the existing schemes will be shown.

In **Table 5**, the accuracy of the proposed scheme is 99.16% in CASIA TIDE v1.0 and 97.52% in CASIA TIDE v2.0. It exceeds the results of other methods in CASIA TIDE v1.0, and is slightly worse than that of [33] and exceeds that of [25], [29] and [31] in CASIA TIDE v2.0. In [31], a scheme based on the steerable pyramid transform and local binary pattern is proposed, which extracts features on single chrominance channel. It ignores the inherent relationships among three channels and so it is in [25] and [40]. Although in [29] QDCT is used, it only selects the magnitude to extract the classification features. This scheme utilizes the inherent relationship among three channels but it neglects the function of phases. From Section 4.2, it can been seen that the performance of phase is near to that of magnitude. Combination features of magnitude and phases possess more integral information of the whole image, so compared with other methods, the proposed scheme has the best performance.

4. Conclusion

In this paper, the correlation among three channels is effectively used. A novel quaternion Markov is proposed to extract classification features in QDCT domain, which consists of global quaternion Markov and local quaternion Markov. Pointing to the magnitude part and the phase part of the proposed quaternion Markov, three different methods are used to process the different arrays and obtain classification features. Meanwhile, in order to wipe off the redundant features, SVMRFE is used to improve the classifcation efficiency of SVM. The final experimental results show that the performance of the proposed scheme is the best compared to the existing schemes. In QDCT domain, strength information is more than texture information. To further obtain intact information of a color image, color quaternion wavelet transform (CQWT) will be used in future. How to extract the combination features in both QDCT and CQWT will be studied.

References

[1] F. Li, C.g Ou, Y. Gui, and L. Xiang, "Instant Edit Propagation on Images Based on Bilateral Gri d, Computers," *Materials & Continua*, 2019. Article (CrossRef Link)

[2] J. Wang, T. Li, X. Luo, Y. Q. Shi, R. Liu and S. K. Jha, "Identifying Computer Generated Images Based on Quaternion Central Moments in Color Quaternion Wavelet Domain," *IEEE Trans. on Circuits & Systems for Video Technol*., 29(9), 2775-2785, 2019. Article (CrossRef Link)

[3] N. Jayashree, R. S. Bhuvaneswaran, "A Robust Image Watermarking Scheme Using Z-Transform, Discrete Wavelet Transform and Bidiagonal Singular Value Decomposition," *CMC-Computers, Materials & Continua*, 58(1), 263–285, 2019. Article (CrossRef Link)

[4] J. Wang, H. Wang, J. Li, X. Luo, Y. Shi and S. K. Jha, "Detecting double JPEG compressed color images with the same quantization matrix in spherical coordinates," *IEEE Trans. on Circuits & Systems for Video Technol*., 2019. Article (CrossRef Link)

[5] J. Li, B. Ma, C. Wang, "Extraction of PRNU Noise from Partly Decoded Video," *Journal of Visual Communication and Image Representation*, 57, 183-191, 2018. Article (CrossRef Link)

[6] C. Wang, X. Wang, Z. Xia, B. Ma, Y. Q. Shi, "Image Description with Polar Harmonic Fourier Moments," *IEEE Transactions on Circuits and Systems for Video Technology*, 2019. Article (CrossRef Link)

[7] Y. Gui and G. Zeng, "Joint learning of visual and spatial features for edit propagation from a sin gle image," *Visual Computer*, 2019. Article (CrossRef Link)

[8] N. S. Rani, M. Chandrajith, B. R. Pushpa, J., B, Bipin Nair, "A Deep Convolutional Architectural Framework for Radiograph Image Processing at Bit Plane Level for Gender & Age Assessment," *CMC-Computers, Materials & Continua*, 62(2), 679–694, 2020. Article (CrossRef Link)

[9] Q. Yin, J. Wang, X. Luo, J. Zhai, S. Jha, Y. Shi, "Quaternion Convolutional Neural Network for Color Image Classification and Forensics," *IEEE Access*, 7(1), 20293-20301, 2019. Article (CrossRef Link)

[10] M. Long, Y. Zeng, "Detecting Iris Liveness with Batch Normalized Convolutional Neural Network," *CMC-Computers, Materials & Continua*, 58(2), 493–504, 2019. Article (CrossRef Link)

[11] D. Hsiao, S. Pei, "Detecting digital tampering by blur estimation," *First Int. Work. Syst. Approaches to Digit. Forensic Eng*., 1, 264–278, 2005. Article (CrossRef Link)

[12] P. Kakar, N. Sudha, W. Ser, "Exposing digital image forgeries by detecting discrepancies in motion blur," *IEEE Trans. Multimed*, 13,443–452, 2013. Article (CrossRef Link)

[13] K. Bahrami, A. Kot, L. Li, H. Li, "Blurred image splicing localization by exposing blur type inconsistency," *IEEE Trans. Inf. Forensic. Secur*., 10, 999–1009, 2015. Article (CrossRef Link)

[14] M. Rao, A. Rajagopalan, G. Seetharaman, "Harnessing motion blur to unveil splicing," *IEEE Trans. Inf. Forensic. Secur*., 9, 583–595, 2014. Article (CrossRef Link)

[15] J. Li, X. Li, B. Yang, X. Sun, "Segmentation-based image copy-move forgery detection scheme," *IEEE Trans. Inf. Forensic. Secur*., 10, 507–518, 2015. Article (CrossRef Link)
[16] Y.-F. Hsu, S.-F. Chang, "Camera response functions for image forensics: an automatic algorithm for splicing detection," *IEEE Trans. Inf. Forensic. Secur*., 5, 816–825, 2010. Article (CrossRef Link)
[17] H. Yao, S. Wang, X. Zhang, C. Qin, J. Wang, "Detecting image splicing based on noise level inconsistency," *Multimed. Tools. Appl*., 1, 1–23, 2016. Article (CrossRef Link)
[18] F. Cao, B. An, J. Wang, D. Ye, H. Wang, "Hierarchical recovery for tampered images based on watermark self-embedding," *Displays*, 46, 5260, 2017. Article (CrossRef Link)
[19] C. Qin, X. Chen, J. Dong, X. Zhang, "Perceptual image hashing with selective sampling for salient structure features," *Displays*, 45, 2637, 2016. Article (CrossRef Link)
[20] H. Farid, S. Lyu, "Higher-order wavelet statistics and their application to digital forensics," *IEEE Work. Stat. Anal. Comput. Vis.*, 8, 94, 2003. Article (CrossRef Link)
[21] D. Fu, Y. Shi, W. Su, "Detection of image splicing based on hilbert-huang transform and moments of characteristic functions with wavelet decomposition," *Digit. Watermarking*, 1, 177–187, 2006. Article (CrossRef Link)
[22] Y. Shi, C. Chen, W. Chen, "A natural image model approach to splicing detection," in *Proc. of 9th Work. Multimed. Secur*., 1, 51–62, 2007. Article (CrossRef Link)
[23] W. Wang, J. Dong, T. Tan, "Effective image splicing detection based on image chroma," in *Proc. of 2009 16th IEEE Inter. Conf. on Image Process*, 5, 1257–1260, 2009. Article (CrossRef Link)
[24] P. Sutthiwan, Y. Shi, H. Zhao, T. Ng, W. Su, "Markovian rake transform for digital image tampering detection," *Trans. data hiding and Multimed. Secur*., VI 1, 1–17, 2011. Article (CrossRef Link)
[25] Z. He, W. Lu, W. Sun, J. Huang, "Digital image splicing detection based on markov features in dct and dwt domain," *Pattern Recognit*, 45, 4292–4299, 2012. Article (CrossRef Link)
[26] E. El-Alfy, M. Qureshi, "Combining spatial and dct based markov features for enhanced blind detection of image splicing," *Pattern Anal. Appl*., 18, 713–723, 2015. Article (CrossRef Link)
[27] E. O. Yildirim and G. Ulutaş, "Image splicing detection with dwt domain extended Markov features," in *Proc. of 2018 26th Signal Processing and Communications Applications Conference (SIU)*, Izmir, 1-4, 2018. Article (CrossRef Link)
[28] T. Ng, S. Chang, Q. Sun, A data set of authentic and spliced image blocks, Columbia University.
[29] C. Li, Q. Ma, L. Xiao, M. Li, A. Zhang, "Image splicing detection based on markov features in qdct domain," *Intel. Comput. Theor. Appl*., 9227, 297–303, 2015. Article (CrossRef Link)
[30] J. Dong, W. Wang, T. Tan, "Casia image tampering detection evaluation database, Signal and Information Processing (ChinaSIP)," in *Proc. of 2013 IEEE China Summit & International Conference on*, 5, 422–426, 2013. Article (CrossRef Link)
[31] G. Muhammad, M. Al-Hammadi, M. Hussain, "Image forgery detection using steerable pyramid transform and local binary pattern," *Mach. Vision Appl*., 25 (4), 985–995, 2014. Article (CrossRef Link)
[32] Q. Zhang, W. Lu, J. Weng, "Joint image splicing detection in dct and contourlet transform domain," *J. Vis. Commun. Image Represent*, 40, 449–458, 2016. Article (CrossRef Link)
[33] Y. Rao, J. Ni, "A deep learning approach to detection of splicing and copymove forgeries in images," *IEEE Int. Work. Inf. Forensics Secur*., 1–6, 2016. Article (CrossRef Link)
[34] E. ODABAŞ YILDIRIM and G. ULUTAŞ, "Markov-Based Image Splicing Detection in the DCT High Frequency Region," in *Proc. of 2018 International Conference on Artificial Intelligence and Data Processing (IDAP)*, Malatya, Turkey, 1-4, 2018. Article (CrossRef Link)
[35] W. Hamilton, "Scientific books: elements of quaternions," *Science*, 14, 65–66, 1901. Article (CrossRef Link)
[36] J. Wang, Y.-Q. T. Li, S.Lian, J.Ye, "Forensics feature analysis in quaternion wavelet domain for distinguishing photographic images and computer graphics," *Multimed. Tools. Appl*., 117, 2016. Article (CrossRef Link)

[37] W. Feng, B. Hu, "Quaternion discrete cosine transform and its application in color template matching," *IEEE Congr. on Image and Signal Process*, 1, 252–256, 2008. Article (CrossRef Link)
[38] C. Yan, Y. Zhang, J. Xu, "A highly parallel framework for hevc coding unit partitioning tree decision on many-core processors," *IEEE Signal Process Lett.*, 21, 573–576, 2014. Article (CrossRef Link)
[39] C. Yan, Y. Zhang, J. Xu, "Efficient parallel framework for hevc motion estimation on many-core processors," *IEEE Trans. Circ. Syst. Video Technol.*, 24, 2077–2089, 2014. Article (CrossRef Link)
[40] X. Zhao, J. Li, S. Li, "Detecting digital image splicing in chroma spaces," *Lect. Notes in Comput. Science*, 6526, 12–22, 2010. Article (CrossRef Link)

Jinwei Wang is a professor from Nanjing University of Information Science & Technology. He received B.S. degree in automatic control from Inner Mongolia University of Technology in 2000. He received Ph.D. in information security at Nanjing University of Science & Technology in 2007 and was a visiting scholar in Service Anticipation Multimedia Innovation (SAMI) Lab of France Telecom R&D Center (Beijing) in 2006. He worked as a senior engineer at the 28th research institute, CETC from 2007 to 2010. He worked as a visiting scholar at New Jersey Institute of Technology, NJ, USA from 2014 to 2015. His research interests include multimedia copyright protection, multimedia forensics, multimedia encryption and data authentication. He has published more than 50 papers, hosted and participated in more than 10 projects.

Renfeng Liu received his B.S. in computer science and technology from Yancheng Teachers University in 2014. He is pursuing M.S. degree in computer science and technology from Nanjing University of Information Science & Technology. His research interests include multimedia forensics.

Hao Wang received his B.S. in IoT engineering from Binjiang College, Nanjing University of Information Science & Technology in 2017. He is pursuing M.S. degree in computer science and technology from Nanjing University of Information Science & Technology. His research interests include multimedia forensics.

Yun-Qing Shi has joined the Department of Electrical and Computer Engineering at the New Jersey Institute of Technology (NJIT), Newark, NJ since 1987, and is currently a professor there. He obtained his B.S. degree and M.S. degree from the Shanghai Jiao Tong University, Shanghai, China; his Ph.D. degree from the University of Pittsburgh, PA. His research interests include multimedia data hiding, forensics and security (robust watermarking, reversible data hiding, authentication, steganography and steganalysis, tampering detection, computer graphics classification from photographic images, camera identification, detection of double JPEG/MPEG compression), visual signal processing and communications (motion analysis, video compression and transmission), applications of image processing, computer vision and pattern recognition to industrial automation and biomedical engineering, theory of multidimensional systems and signal processing (robust stability of linear systems, 2-D spectral factorization, 2-D/3-D interleaving).